Epigenetics & Chromatin

RESEARCH Open Access

H3.3K122A results in a neomorphic phenotype in mouse embryonic stem cells

Benjamin J. Patty[1], Cailin Jordan[1,2], Santana M. Lardo[1], Kris Troy[1,3] and Sarah J. Hainer[1,4*]

Abstract

Canonical histone H3 and histone variant H3.3 are posttranslationally modified with the genomic distribution of these marks denoting different features and these modifications may influence transcription. While the majority of posttranslational modifications occur on histone tails, there are defined modifications within the globular domain, such as acetylation of H3K122/H3.3K122. To understand the function of the amino acid H3.3K122 in transcriptional regulation, we attempted to generate H3.3K122A mouse embryonic stem (mES) cells but were unsuccessful. Through multi-omic profiling of mutant cell lines harboring two or three of four H3.3 targeted alleles, we have uncovered that H3.3K122A is neomorphic and results in lethality. This is surprising as prior studies demonstrate H3.3-null mES cells are viable and pluripotent but exhibit a reduced differentiation capacity. Together, these studies have uncovered a novel dependence of a globular domain residue within H3.3 for viability and broadened our understanding of how histone variants contribute to transcription regulation and pluripotency in mES cells.

Introduction

Individual canonical histone proteins within a nucleosome can be substituted with histone variants (reviewed in [1]), which play important roles in chromatin dynamics during DNA-templated activities [1, 2]. Variant histone proteins for each of the four canonical histone proteins have been identified, with among the most well studied being histone variant H3.3, which replaces canonical histone H3. In mammals, there are two genes that encode H3.3: *H3f3a* and *H3f3b* [2]. *H3f3a* and *H3f3b* encode an identical polypeptide sequence, but exhibit allele-specific gene structures, nucleic acid sequences, expression patterns, and have different requirements during development [3–6]. The amino acid sequence of variant H3.3 is very similar to that of canonical H3.1 and H3.2, with only five differing amino acids [1]. H3.3 has a context-specific relationship with transcription, and is found at regions of active transcription such as enhancers and regions of heterochromatin including telomeres and other repetitive regions of the genome [7–10]. The context specific role of H3.3 is mediated by distinct histone chaperone systems and posttranslational modifications: the HIRA complex incorporates H3.3 into euchromatin where it receives transcription-associated modifications, while the nucleosome remodeler ATRX and histone chaperone DAXX incorporate H3.3 into heterochromatic regions where it receives modifications associated with repression [8, 9, 11–13]. At these locations, H3.3 regulates the turnover of nucleosomes to promote proper transcription factor (TF) binding and/or maintenance of histone modifications to preserve the local chromatin state [14–17]. In murine embryonic stem cells (mES cells), H3.3 is dispensable for viability and regulation of pluripotency, but is required

*Correspondence:
Sarah J. Hainer
sarah.hainer@pitt.edu
[1]Department of Biological Sciences, University of Pittsburgh, Pittsburgh, PA, USA
[2]Basic Sciences Division, Fred Hutchinson Cancer Center, Seattle, WA, USA
[3]Molecular, Cellular, and Developmental Biology Department, University of California Santa Barbara, Santa Barbara, CA, USA
[4]UPMC Hillman Cancer Center, University of Pittsburgh, Pittsburgh, PA, USA

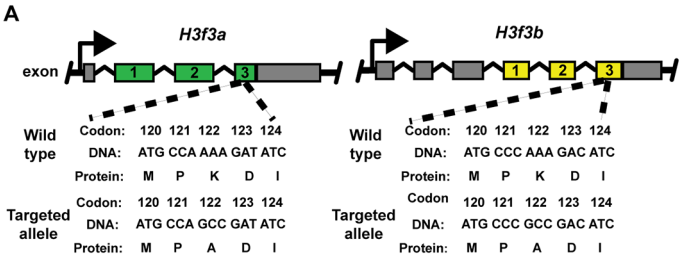

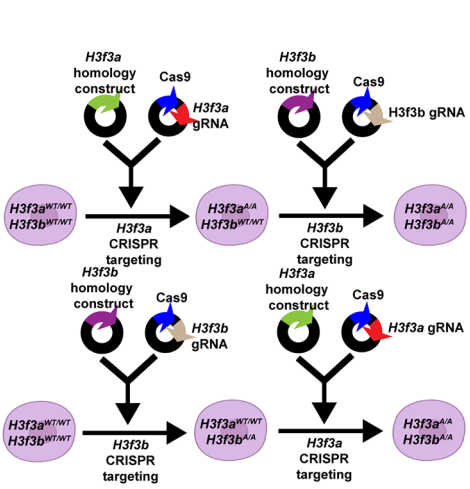

C

Genotype of targeted cell line	Media conditions	Target	Number of screened clones	Percent homozygous	Percent heterozygous	Percent untargeted
H3f3a$^{WT/WT}$ *H3f3b*$^{WT/WT}$	LIF+serum	*H3f3a*	100	12%	44%	44%
H3f3a$^{WT/WT}$ *H3f3b*$^{WT/WT}$	LIF+serum	*H3f3b*	264	23%	57%	20%
H3f3a$^{A/A}$ *H3f3b*$^{WT/WT}$	LIF+serum	*H3f3b*	263	0%	18%	82%
H3f3a$^{WT/WT}$ *H3f3b*$^{A/A}$	LIF+serum	*H3f3a*	234	0%	39%	61%
H3f3a$^{A/A}$ *H3f3b*$^{WT/WT}$	LIF/2i+serum	*H3f3b*	256	0%	35%	65%

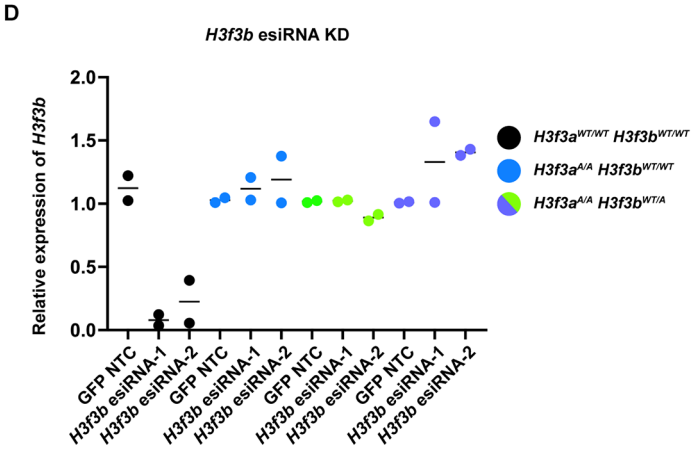

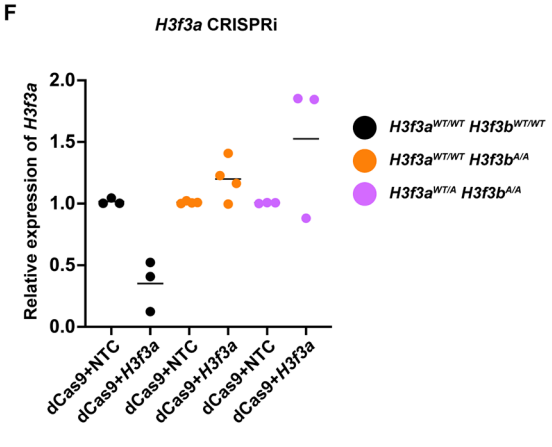

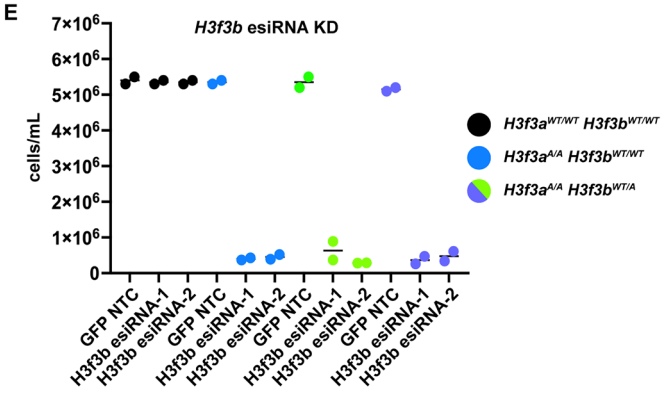

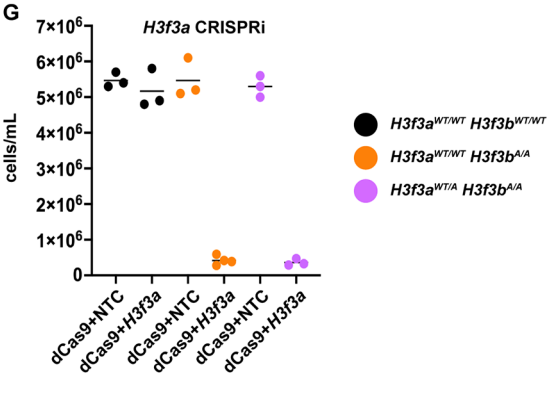

Fig. 1 (See legend on next page.)

(See figure on previous page.)

Fig. 1 H3.3K122A mutation may be lethal in ES cells. **A**. Schematic of *H3f3a* (left) and *H3f3b* (right) loci, with wildtype and targeted DNA sequences denoted. **B**. Schematic of two-step targeting method to generate H3.3K122A cell lines. **C**. Table summarizing the mES cell clones screened to generate single targeted cell lines (top two rows) and dual targeted cell lines (bottom four rows). "Media conditions" indicates the media formulation used during targeting. A full description of clones screened can be found in the Methods and in Supplemental Table 1. **D**. RT-qPCR results of esiRNA knockdowns targeting *H3f3b* or GFP non-template control (NTC) in wildtype cell lines (control for KD efficiency), $H3f3a^{A/A}H3f3b^{WT/WT}$ cell lines, and $H3f3a^{A/A}H3f3b^{WT/A}$ cell lines. Each point is an independent biological replicate. The line represents the average of biological replicates. **E.** Number of viable cells for esiRNA knockdowns targeting *H3f3b* or GFP non-template control (NTC) in wildtype cell lines (control for KD efficiency), $H3f3a^{A/A}H3f3b^{WT/WT}$ cell lines (parental), and $H3f3a^{A/A}H3f3b^{WT/A}$ cell lines. Each point is an independent biological replicate. The line represents the average of biological replicates. **F**. As in D, for RT-qPCR results of CRISPRi targeting of *H3f3a* or non-template control (NTC) in wildtype cell lines (control for efficiency), $H3f3a^{WT/WT}H3f3b^{A/A}$ cell lines (parental), and $H3f3a^{WT/A}H3f3b^{A/A}$ cell line. **G**. As in **E**, for CRISPRi targeting of *H3f3a* or non-template control (NTC) in wildtype cell lines (control for efficiency), $H3f3a^{WT/WT}H3f3b^{A/A}$ cell lines (parental), and $H3f3a^{WT/A}H3f3b^{A/A}$ cell lines

for differentiation and transitions between cell states [10, 13, 18, 19].

Active enhancers are characterized by distinct chromatin features, including flanking nucleosomes marked by H3K4me1 and H3K27ac [20, 21]. However, beyond these well-established histone modifications, there are additional modifications that are less well characterized. K122 is a residue found in both H3 and H3.3 at the nucleosome dyad and can be acetylated in mammalian cells and fission yeast (H3K122ac) [22]. In vitro, H3K122ac reduces histone/DNA interactions by destabilizing nucleosomes [23]. Though budding yeast lack H3K122ac, H3K122A, H3K122R, and H3K122Q mutations reduce nucleosome occupancy over highly transcribed genes and result in reduced telomeric, ribosomal, and HML silencing [24, 25]. Finally, the Bickmore lab found that, in mES cells and MCF-7 human cells, H3K122ac marks a subset of enhancers, sometimes without H3K27ac [26]. Together, these data suggest an important role for H3K122 in cells, with the implication that acetylation may stimulate transcription. However, to date, there has been no study dissecting how H3.3 and K122ac may coordinate to regulate transcription.

To examine the role of H3.3K122 in mES cells, we attempted to generate mES cells containing *H3f3a* and *H3f3b* K122A homozygous mutations. In addition to altering residue charge and size, a mutation that replaces the lysine residue with an alanine (H3.3K122A) would prevent acetylation (H3.3K122ac) as alanine residues are not readily acetylated. Despite many attempts to generate mES cells where all four H3.3 alleles contain the K122A mutation, we were unable to recover these cell lines, suggesting lethality. We succeeded in generating cell lines containing either two or three of the four H3.3 alleles with the K122A mutation. We were unable to deplete the expression of the remaining wildtype H3.3 within these cell lines, supporting that having H3.3K122A as the sole H3.3 protein results in lethality. Despite this, to investigate the impact of H3.3K122A on mES cell biology, we characterized cell lines containing two or three alleles with the H3.3K122A mutation. We found that with an increasing number of H3.3K122A alleles, the phenotypic, transcriptomic, and epigenomic defects are intensified. Together, these studies suggest that K122 (and perhaps K122ac) is critical to proper H3.3 function in mES cells.

Results

H3.3K122A may be lethal in mES cells

While *H3f3a* and *H3f3b* encode the same polypeptide, the gene structures and coding sequences of *H3f3a* and *H3f3b* are distinct (Fig. 1A). Therefore, we used a two-step targeting strategy to generate mutations in *H3f3a* and *H3f3b*. First, we independently targeted either *H3f3a* or *H3f3b* using CRISPR/Cas9-directed homologous recombination to replace the endogenous sequence with a mutation resulting in a single codon change to alter lysine 122 to alanine (K122A; Fig. 1B). We were able to generate homozygous single targeted cell lines ($H3f3a^{A/A}H3f3b^{WT/WT}$ or $H3f3a^{WT/WT}H3f3b^{A/A}$) with reasonable frequency (Fig. 1C and Supplemental Table 1). Sequence-confirmed $H3f3a^{A/A}H3f3b^{WT/WT}$ and $H3f3a^{WT/WT}H3f3b^{A/A}$ cell lines (referred to as single targeted) were then independently targeted for the opposite H3.3 encoding gene, with the goal of generating cell lines containing all four alleles with the K122A mutation (Fig. 1B and Supplemental Table 1). Despite multiple attempts at generating $H3f3a^{A/A}H3f3b^{A/A}$ cell lines in both LIF/serum and 2i+LIF/serum media, we were unable to generate these clones (Fig. 1C and Supplemental Table 1). However, we did obtain dual targeted (either $H3f3a^{WT/A}H3f3b^{A/A}$ or $H3f3a^{A/A}H3f3b^{WT/A}$) cell lines where three of the four alleles are mutated to alanine (Fig. 1C and Supplemental Table 1).

Given these results, we hypothesized that $H3f3a^{A/A}H3f3b^{A/A}$ may be lethal in mES cells. To test this, we attempted to deplete remaining wildtype H3.3 using esiRNAs or CRISPRi in single targeted ($H3f3a^{WT/WT}H3f3b^{A/A}$ or $H3f3a^{A/A}H3f3b^{WT/WT}$) and dual targeted ($H3f3a^{WT/A}H3f3b^{A/A}$ or $H3f3a^{A/A}H3f3b^{WT/A}$) cell lines. We designed and tested two independent sets of esiRNAs targeting *H3f3b* and transfected these into wildtype, $H3f3a^{A/A}H3f3b^{WT/WT}$, or $H3f3a^{A/A}H3f3b^{WT/A}$ cell lines using esiRNAs targeting *GFP* as an unexpressed non-template control (NTC). After 48 h, we observed 85–95% depletion of *H3f3b* in wildtype cells using either set of *H3f3b*-targeting esiRNAs, yet no

depletion of *H3f3b* in cell lines harboring $H3f3a^{A/A}$ and $H3f3b^{WT/WT}$ or $H3f3b^{WT/A}$ (Fig. 1D). We believe this is due to lethality upon successful *H3f3b* depletion in these cell lines, as we observed a ~ 10-fold reduction in viable cells in $H3f3a^{A/A}$ and $H3f3b^{WT/WT}$ or $H3f3b^{WT/A}$ relative to $H3f3a^{WT/WT}H3f3b^{WT/WT}$ and $H3f3a^{WT/A}H3f3b^{WT/WT}$ cell lines (Fig. 1E). Because we were unable to design unique esiRNAs targeting *H3f3a* that resulted in depletion, we generated sgRNAs targeting *H3f3a* and performed CRISPRi in wildtype, $H3f3a^{WT/WT}H3f3b^{A/A}$, and $H3f3a^{WT/A}H3f3b^{A/A}$ cell lines (Fig. 1F). We observed ~ 55% depletion of *H3f3a* only in wildtype cells, but no depletion of *H3f3a* in cell lines harboring $H3f3b^{A/A}$ (Fig. 1F). Similar to *H3f3b* esiRNA targeting, CRISPRi targeting of *H3f3a* in $H3f3a^{WT/WT}H3f3b^{A/A}$ and $H3f3a^{WT/A}H3f3b^{A/A}$ cells resulted in an approximate 10-fold reduction in abundance of viable cells relative to controls (Fig. 1G). Together with our inability to generate $H3f3a^{A/A}H3f3b^{A/A}$ clones, these results suggest that the H3.3K122A mutation at all four H3.3 alleles may be lethal in mES cells. These results are surprising as it has been previously shown that H3.3 KO mES cells and mES cells depleted of H3.3 are viable [10, 18]. Therefore, to further understand the role of H3.3K122 in mES cells, we characterized cell lines containing either two or three of the H3.3 alleles successfully targeted for H3.3K122A.

H3.3K122A results in reduced pluripotency and slow growth in mES cells

To understand how the H3.3K122A mutation impacts mES cell biology, we assessed whether mES cell pluripotency was disrupted using alkaline phosphatase (AP) staining (Fig. 2A, Supplemental Fig. 1A). AP is a membrane-bound protein highly expressed in mES cells, and is commonly used as a phenotypic proxy for pluripotency [27]. All mutant cell lines displayed reduced AP staining relative to wildtype, with $H3f3a^{A/A}$ or $H3f3a^{WT/A}$ containing cell lines showing slightly less staining relative to $H3f3a^{WT/WT}$ containing cell lines (Fig. 2A, Supplemental Fig. 1A). We next performed a 6-day growth assay with wildtype and mutant cell lines (Fig. 2B, Supplemental Fig. 1B-D). Though all mutant cell lines had a minor reduction in growth by day 6 relative to wildtype, $H3f3a^{A/A}$ containing cell lines had a more consistent and severe growth defect relative to $H3f3a^{WT/WT}$ or $H3f3a^{WT/A}$ containing cell lines (Fig. 2B, Supplemental Fig. 1B-D). These data support a previous study arguing that *H3f3a* is evolutionarily specialized for transcriptional programs associated with cell proliferation [5]. Together, these observations may suggest allele-specific requirements in the functions of H3.3K122 related to cell proliferation and regulation of pluripotency, with *H3f3a* having a more prominent role in mES cells.

H3.3K122A mES cells have reduced levels of H3.3

We next examined the protein levels of H3, H3.3, and K122ac (antibody recognizes both H3K122ac and H3.3K122ac) in each cell line and observed little change in H3 and K122ac abundance (Fig. 3A-B). Interestingly, all *H3f3a*-targeted cell lines ($H3f3a^{WT/A}$ or $H3f3a^{A/A}$) exhibited a modest reduction in H3.3 abundance (~ 60–70% of WT levels) while the $H3f3a^{WT/WT}H3f3b^{A/A}$ lines had little or no reduction (Fig. 3A-B). We performed total and nascent RT-qPCR and found that all cell lines exhibited similar levels of *H3f3a* but found the $H3f3b^{A/A}$ cell lines exhibited reduced expression and transcription of *H3f3b* (Supplemental Fig. 1E-F).

H3.3K122A cells display no major changes in H3.3 euchromatic occupancy

Given our finding that total H3.3 protein abundance is reduced in the H3.3K122A mutant cell lines, we examined whether H3.3 chromatin occupancy is altered. To that end, we performed Cleavage Under Target and Release Using Nuclease (CUT&RUN) for H3.3 in wildtype mES cells and each single/dual targeted cell line, with high reproducibility between replicates and across cell lines (Supplemental Fig. 1G).

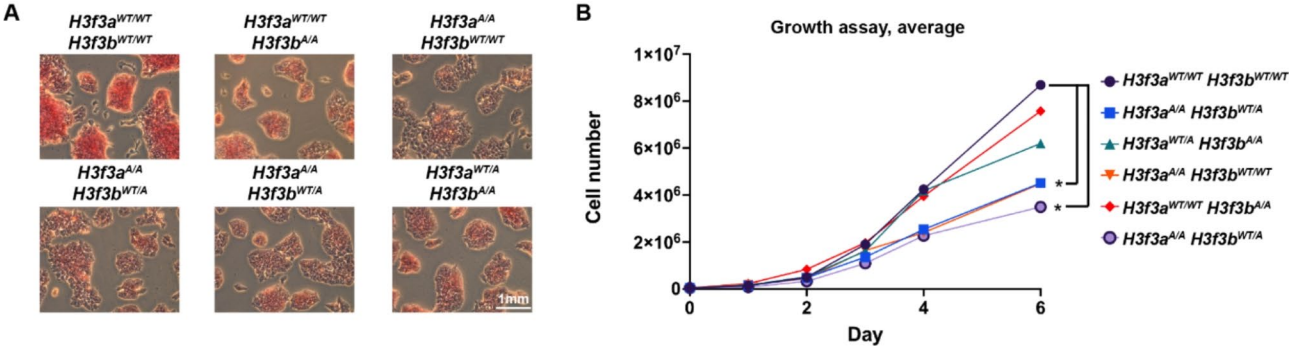

Fig. 2 H3.3K122A cell lines have reduced AP staining and growth relative to wildtype cells. **A**. Alkaline phosphatase (AP) staining of wildtype and H3.3K122A cell lines. Shown are representative images from one of three biological replicates. **B**. Growth curve for WT and H3.3K122A cell lines with live cell numbers quantified on 1, 2, 3, 4, and 6 days post plating. Graph represents the average of 3 biological replicates

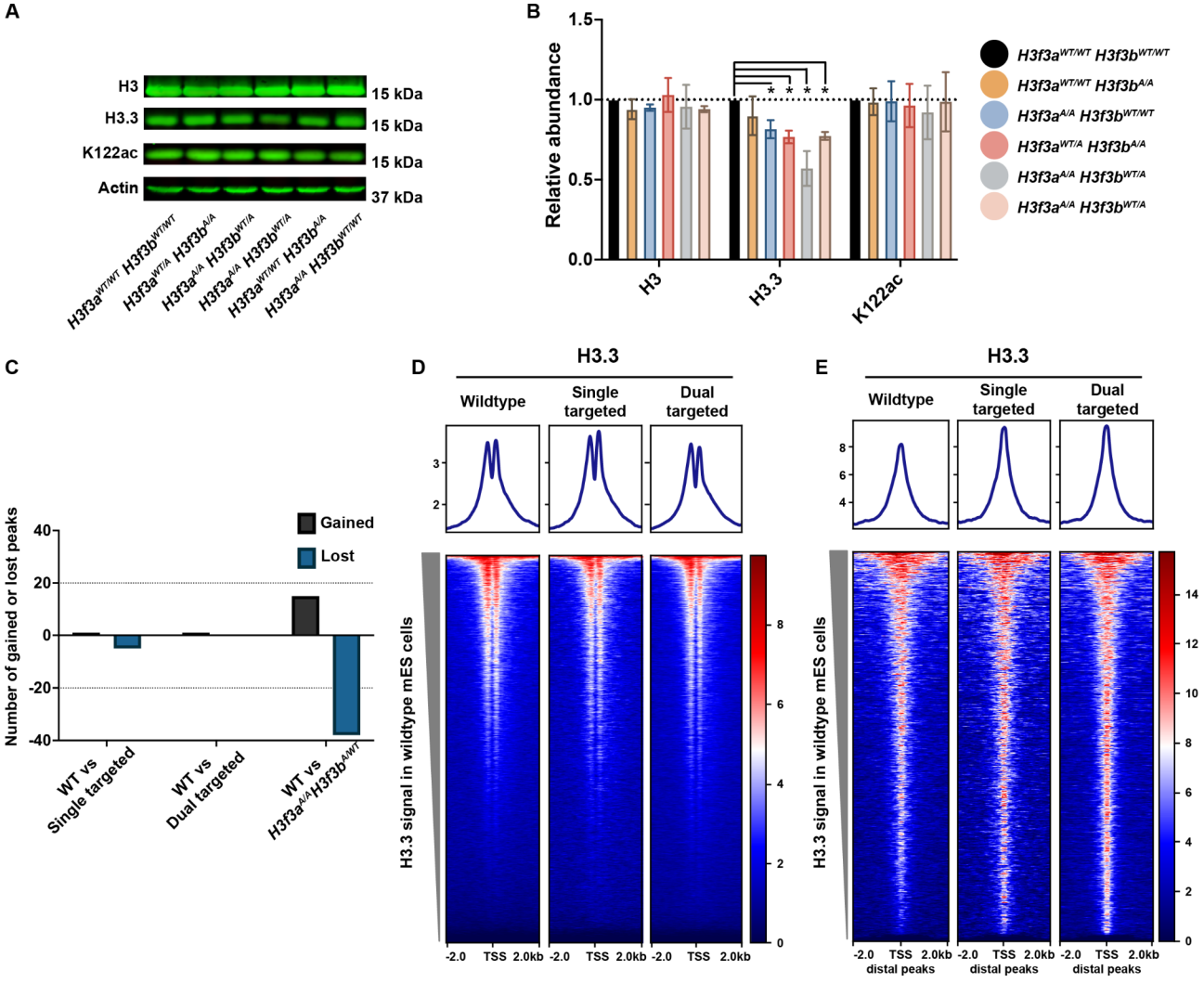

Fig. 3 H3.3K122A cell lines have reduced H3.3 protein levels relative to wildtype cells but not reduced H3.3 chromatin occupancy. **A**. Western blot analysis for total H3, H3.3, and K122ac in wildtype and H3.3K122A cell lines. Actin is used as a loading control. **B**. Quantification of three biological replicates for each western blot in A. *p value ≤ 0.05, two sided T-test. **C**. Differentially enriched H3.3 CUT&RUN peaks (|LFC|≥0.5 and FDR ≤ 0.05) in the single targeted and dual targeted cell lines relative to wildtype. Black indicates number of gained peaks, and blue indicates number of lost peaks. **D**. Metaplots and heatmaps visualizing average H3.3 enrichment over TSSs in wildtype ($n=2$), single targeted ($n=2$), and dual targeted cell lines ($n=3$). $N=22{,}598$ loci. **E**. As in F, for gene distal H3.3 peaks. $N=3{,}347$ loci

We defined 5,447 H3.3 consensus peaks across the datasets (excluding repetitive regions) yet found less than 60 H3.3 peaks with differential enrichment in all comparisons to wildtype (Fig. 3C). This implies that, while the targeted cell lines have modestly reduced protein abundance of total H3.3 relative to wildtype, these cell lines have maintained similar levels of H3.3 within chromatin. Visualization of H3.3 enrichment at transcription start sites (TSSs) and H3.3 gene distal peaks showed similar enrichment in wildtype, single targeted, and dual targeted cell lines, supporting the peak-based analysis (Fig. 3D-E).

Severity of transcription changes in H3.3K122A mutants increases with number of alleles targeted

To understand how H3.3K122A impacts the mES cell transcriptome, we performed the nascent RNA sequencing method Transient Transcriptome sequencing (TT-seq [28]) in wildtype and H3.3K122A targeted cell lines with high reproducibility across replicates (Supplemental Fig. 2A). When comparing the single targeted ($H3f3a^{A/A}H3f3b^{WT/WT}$ and $H3f3a^{WT/WT}H3f3b^{A/A}$) cell lines to wildtype, we observed hundreds of genes with transcriptional changes, with 136 downregulated and 189 upregulated genes (Fig. 4A). However, when comparing dual targeted ($H3f3a^{A/A}H3f3b^{WT/A}$

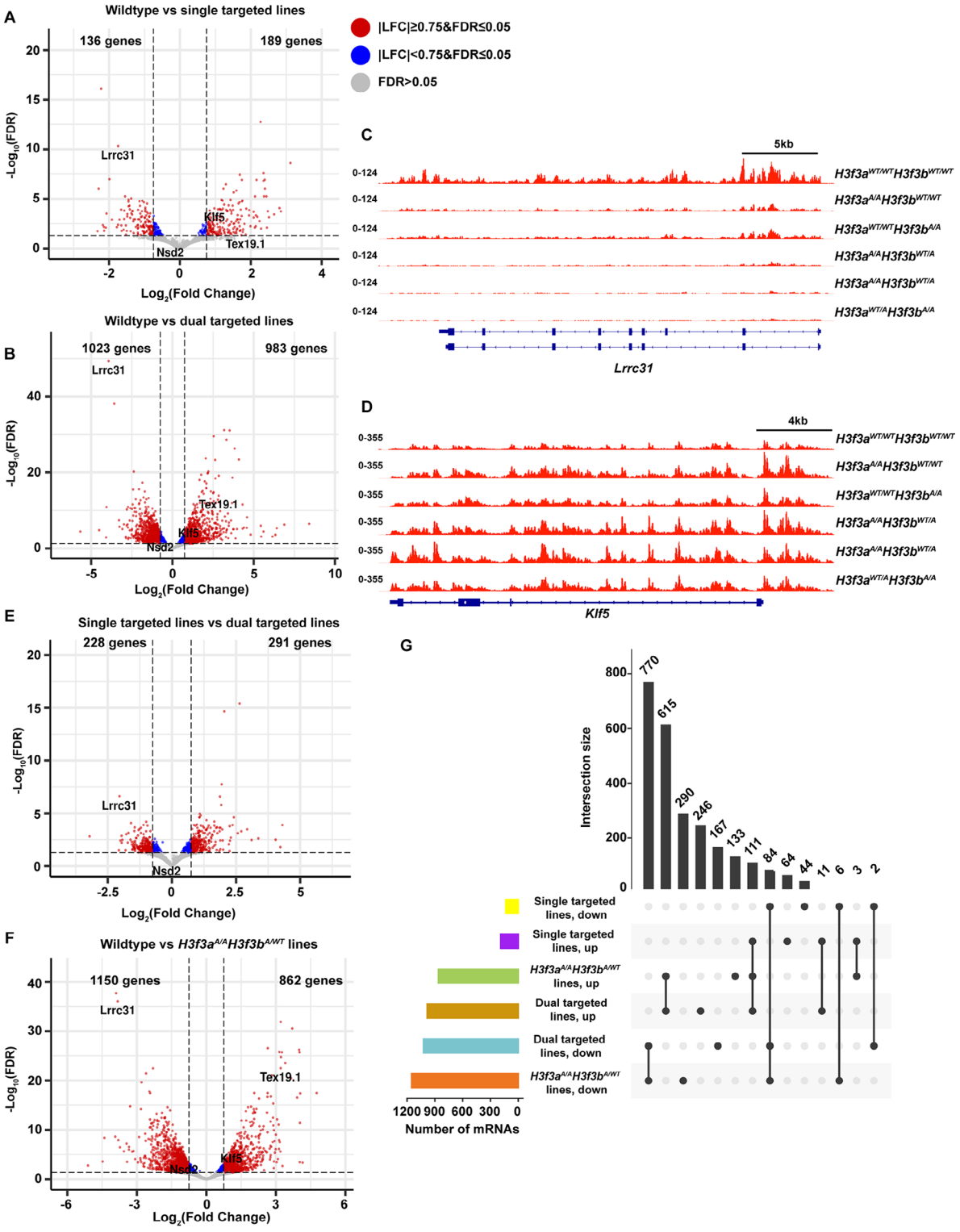

Fig. 4 H3.3K122A results in transcriptomic changes in mES cells. **A**. Volcano plot of differentially transcribed genes in single targeted H3.3K122A cells ($H3f3a^{A/A}H3f3b^{WT/WT}$ and $H3f3a^{WT/WT}H3f3b^{A/A}$, $n=2$) relative to wildtype ($n=3$). Red points are genes |LFC|≥0.75 and FDR ≤ 0.05, blue points are genes |LFC|<0.75 and FDR ≤ 0.05, and grey points are not significantly changed. **B**. As in A, for dual targeted lines ($H3f3a^{A/A}H3f3b^{A/WT}$ and $H3f3a^{A/WT}H3f3b^{A/A}$, $n=3$) relative to wildtype ($n=3$). **C**. Browser track of nascent RNA-seq (TT-seq) from H3.3K122A cell lines and wildtype cells over the *Lrrc31* locus. **D**. As in E, for the *Klf5* locus. **E**. As in A, for dual targeted ($n=3$) relative to single targeted cell lines ($n=2$). **F**. As in A, for $H3f3a^{A/A}H3f3b^{A/WT}$ lines ($n=2$) relative to wildtype ($n=3$). **G**. Upset plot showing the number of differentially transcribed genes ($\log_2$(FC) ≥ 0.75 and FDR ≤ 0.05) shared between genotypes (upper bar graph, black) and the overall number of differentially transcribed genes in each genotype (lower left bar graph)

and *H3f3a*$^{WT/A}$*H3f3b*$^{A/A}$) cell lines to wildtype, we detected thousands of genes with altered transcription (1023 downregulated and 983 upregulated; Fig. 4B). We selected a panel of genes upregulated (*Klf5* and *Tex19.1*) and downregulated (*Nsd2* and *Lrcc31*) and validated these trends with nascent and total RT-qPCR in all targeted cell lines (Supplemental Fig. 2B-E). Visual comparison of TT-seq data across the *Lrrc31* and *Klf5* locus in wildtype and mutant cell lines further validated these trends and indicate a relationship between the severity of transcriptional changes and the number of K122A targeted H3.3 alleles in the genetic background (Fig. 4C-D). We compared changes in transcription between the single and dual targeted cell lines, observing an intermediate number of genes with altered transcription, as expected with increasing severity due to increased K122A alleles (Fig. 4E). Since we performed TT-seq on two clones with identical genotypes (*H3f3a*$^{A/A}$*H3f3b*$^{WT/A}$), we also compared the *H3f3a*$^{A/A}$*H3f3b*$^{WT/A}$ dual targeted lines relative to wildtype and found 1150 downregulated and 862 upregulated genes (Fig. 4F).

We next compared how these differentially transcribed genes compared across single targeted (*H3f3a*$^{A/A}$*H3f3b*$^{WT/WT}$ and *H3f3a*$^{WT/WT}$*H3f3b*$^{A/A}$) and dual targeted cell lines, where we examined dual targeted as either *H3f3a*$^{A/A}$*H3f3b*$^{WT/A}$ only (two cell lines) or *H3f3a*$^{A/A}$*H3f3b*$^{WT/A}$ and *H3f3a*$^{WT/A}$*H3f3b*$^{A/A}$ (three cell lines; Fig. 4G). Moving forward, we will distinguish these genotypes as dual targeted when referring to results combined from *H3f3a*$^{A/A}$*H3f3b*$^{WT/A}$ and *H3f3a*$^{WT/A}$*H3f3b*$^{A/A}$ and as *H3f3a*$^{A/A}$*H3f3b*$^{WT/A}$ when referring to results from these cell lines only.

When comparing the dual targeted vs. *H3f3a*$^{A/A}$*H3f3b*$^{WT/A}$ differentially transcribed genes we found that the dual targeted vs. wildtype had 246 upregulated and 167 downregulated genes uniquely altered relative to *H3f3a*$^{A/A}$*H3f3b*$^{WT/A}$ (Fig. 4G). These unique differentially transcribed genes therefore likely stem from the *H3f3a*$^{WT/A}$*H3f3b*$^{A/A}$ line, thus allowing an opportunity to examine allele-specific effects. To that end, we performed gene ontology (GO) on the overlapping and unique gene sets from the *H3f3a*$^{A/A}$*H3f3b*$^{WT/A}$ vs. wildtype and dual targeted vs. wildtype comparisons (Supplemental Fig. 2F). Genes upregulated and downregulated in both comparisons were enriched in terms related to metabolism and lineage commitment toward vasculogenesis. Genes uniquely downregulated in the *H3f3a*$^{A/A}$*H3f3b*$^{WT/A}$ lines were enriched for processes related to neuronal lineage commitment, while uniquely upregulated genes were associated with epithelial lineage commitment. Together, these studies further support allele-specific requirements for *H3f3a* and *H3f3b*.

Dual targeted cell lines exhibit strong K27ac and subtle K122ac enrichment changes relative to single targeted or wildtype mES cells

To evaluate how the H3.3K122A mutation influences the epigenome of mES cells, we examined the enrichment of K27ac (antibody recognizes both H3K27ac and H3.3K27ac) and K122ac (antibody recognizes both H3K122ac and H3.3K122ac) using CUT&RUN in wildtype and each single targeted and dual targeted line generating datasets with high reproducibility (Supplemental Fig. 3A, B). For K122ac, we found fewer than 100 peaks with differential enrichment in the single targeted or dual targeted lines relative to wildtype (Fig. 5A). For K27ac, we observed few differentially enriched peaks in the single targeted cell lines, hundreds in dual targeted cell lines relative to wildtype, and thousands when comparing *H3f3a*$^{A/A}$*H3f3b*$^{WT/A}$ lines to wildtype (Fig. 5A). Notably, these data follow a similar trend to the observed transcriptomic changes (Fig. 4), with increasing severity as more targeted alleles are present, especially when *H3f3a* is mutated at both alleles.

We next examined K122ac and K27ac enrichment over our consensus K27ac CUT&RUN peaks and K122ac peaks called from published ChIP-seq datasets [26] in wildtype, single targeted, and dual targeted cell lines. We found that while wildtype and single targeted cell lines had comparable levels of K27ac enrichment, the dual targeted cell lines exhibited higher levels of K27ac over consensus peaks (Fig. 5B). Notably, both single and dual targeted cell lines exhibited lower levels of K122ac over K122ac ChIP-seq peaks relative to wildtype (Fig. 5C). As we predicted that the targeted cell lines would have reduced abundance and chromatin incorporation of H3.3K122ac, but the K122ac antibody does not distinguish H3.3K122ac from H3K122ac, these findings suggest that H3.3K122ac may represent a fraction of the global K122ac found in mES cells.

K27ac, K122ac, and H3.3 levels over promoters and gene bodies reflect transcription changes in targeted cell lines

We next examined how H3K27ac enrichment changes in the *H3f3a*$^{A/A}$*H3f3b*$^{WT/A}$ lines might relate to the transcription defects observed. Specifically, we compared K27ac, K122ac, and H3.3 enrichment in the *H3f3a*$^{A/A}$*H3f3b*$^{WT/A}$ lines and wildtype mES cells at the promoters of genes with significantly changed transcription quantified in our TT-seq datasets. Prior studies demonstrate that H3/H3.3 acetylation at promoters and over protein coding gene bodies generally correlates with transcription levels and changes in gene expression [29–32]. Reflecting the transcription changes, the promoters and gene bodies of upregulated genes exhibited increased K27ac and a modest increase in K122ac in *H3f3a*$^{A/A}$*H3f3b*$^{WT/A}$ lines relative to wildtype, while

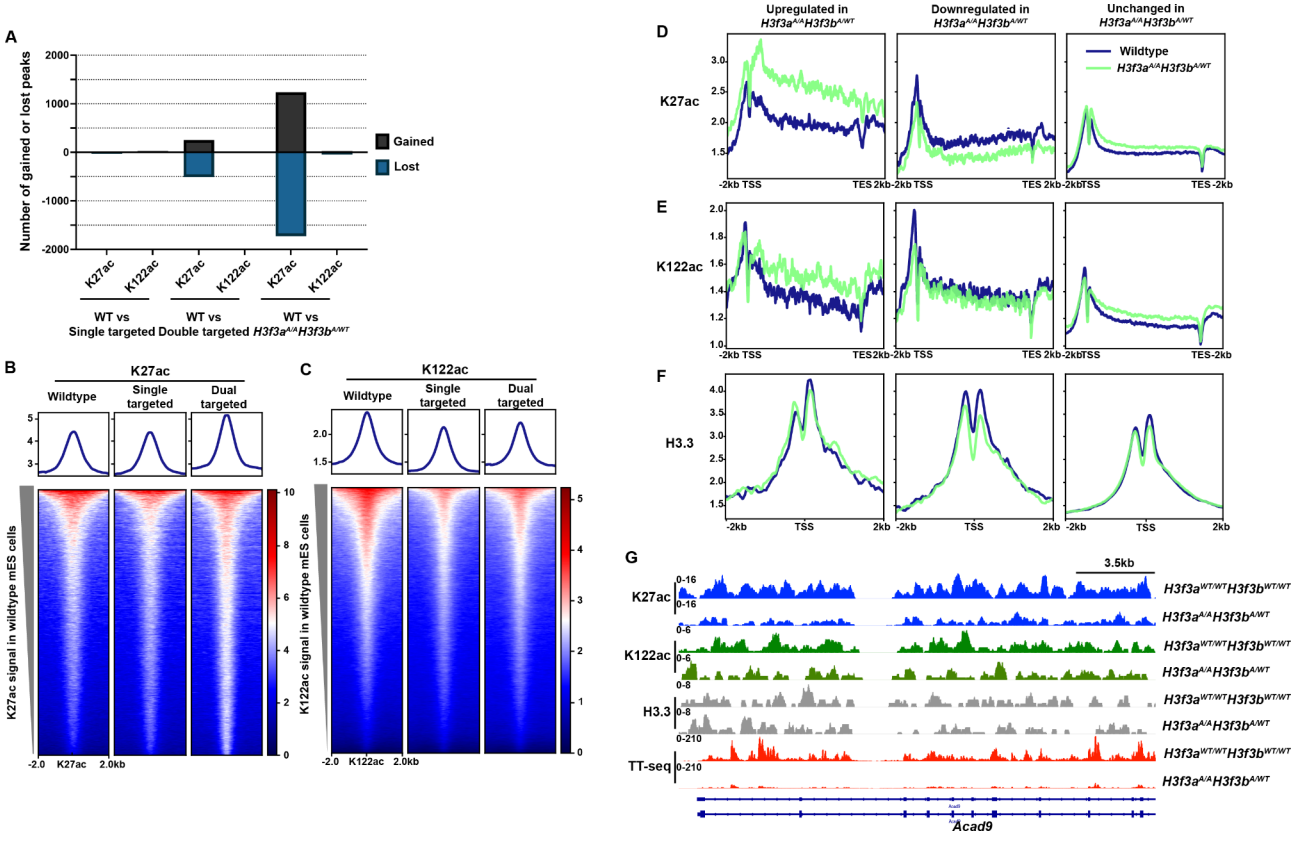

Fig. 5 *H3f3a*$^{A/A}$*H3f3b*$^{A/WT}$ cell lines exhibit altered patterns of K27ac enrichment relative to wildtype mES cells. **A**. Bar graph depicting the number of differentially enriched K27ac or K122ac CUT&RUN peaks (|LFC|≥0.5 and FDR ≤ 0.05) for the indicated cell line comparisons. **B**. Enrichment of K27ac CUT&RUN signal in average wildtype ($n=2$), single targeted ($n=2$), and dual targeted cell lines ($n=3$) over K27ac consensus peaks (this study). **C**. Enrichment of K122ac CUT&RUN signal over average wildtype ($n=2$), single targeted ($n=2$), and dual targeted cell lines ($n=3$) over K122ac consensus peaks called using previously published H3K122ac ChIP-seq data [26]. **D**. Metaplots of K27ac enrichment over genes upregulated, downregulated, or unchanged in *H3f3a*$^{A/A}$*H3f3b*$^{A/WT}$ cell lines. **E**. As in D, for K122ac enrichment. **F**. As in D, for H3.3 enrichment. **G**. Browser track showing replicate averaged enrichment of K27ac (blue), K122ac (green), H3.3 (grey), and sense nascent transcription (red) over the 5′ end of the *Acad9* locus in *H3f3a*$^{A/A}$*H3f3b*$^{A/WT}$ and wildtype mES cells

downregulated genes have decreased enrichment of both marks over promoters and gene bodies (Fig. 5D-E). In *H3f3a*$^{A/A}$*H3f3b*$^{WT/A}$ cell lines, upregulated genes exhibited similar levels in H3.3 enrichment at their promoters relative to wildtype while downregulated genes exhibited a modest reduction in H3.3 enrichment consistent with decreased expression (Fig. 5F). Visual comparison of K27ac, K122ac, H3.3, and nascent transcription in the *H3f3a*$^{A/A}$*H3f3b*$^{WT/A}$ and wildtype mES cells over the *Acad9* and *Adam19* loci exemplify these trends (Fig. 5G and Supplemental Fig. 3C). Previous studies found that K122ac is enriched at bivalent genes [26]. Using a recently curated list of 8,789 bivalently marked loci in mES cells [57], we compared H3.3, K27ac, and K122ac levels in the single or dual targeted cell lines relative to wildtype (Supplemental Fig. 3D-F). We observe modest differences in these marks. Therefore, the H3.3K122A mutation alters transcription in mES cells and H3 acetylation and H3.3 enrichment at promoters and over protein coding gene bodies reflect these transcription changes.

H3.3K122A leads to epigenetic changes over putative enhancer regions involved in regulation of cell fate

To examine the TSS distal effects of the H3.3K122A mutation, we determined the genomic locations of the gained and lost K27ac peaks in the *H3f3a*$^{A/A}$*H3f3b*$^{WT/A}$ cell lines. Interestingly, while 44% of lost K27ac peaks were associated with promoters, only ~6% of gained K27ac peaks were promoter-associated (Fig. 6A, B). Rather, 38%, 25%, and 14% of gained K27ac peaks were annotated as exonic, intronic, and intergenic, respectively, showing that the majority of regions with increased K27ac in the *H3f3a*$^{A/A}$*H3f3b*$^{WT/A}$ lines are TSS distal (Fig. 6A, B). Therefore, we compared the enrichment of K27ac, K122ac, and H3.3 over gained, lost, and unchanged TSS distal K27ac peaks in wildtype and *H3f3a*$^{A/A}$*H3f3b*$^{WT/A}$ lines (Fig. 6C-E). Gained and lost peaks show enrichment of K27ac, K122ac, and H3.3 in either wildtype or *H3f3a*$^{A/A}$*H3f3b*$^{WT/A}$ mES cells, with lost K27ac exhibiting higher levels of K27ac, K122ac, H3.3, and chromatin accessibility (from a wildtype ATAC-seq dataset [56]) in

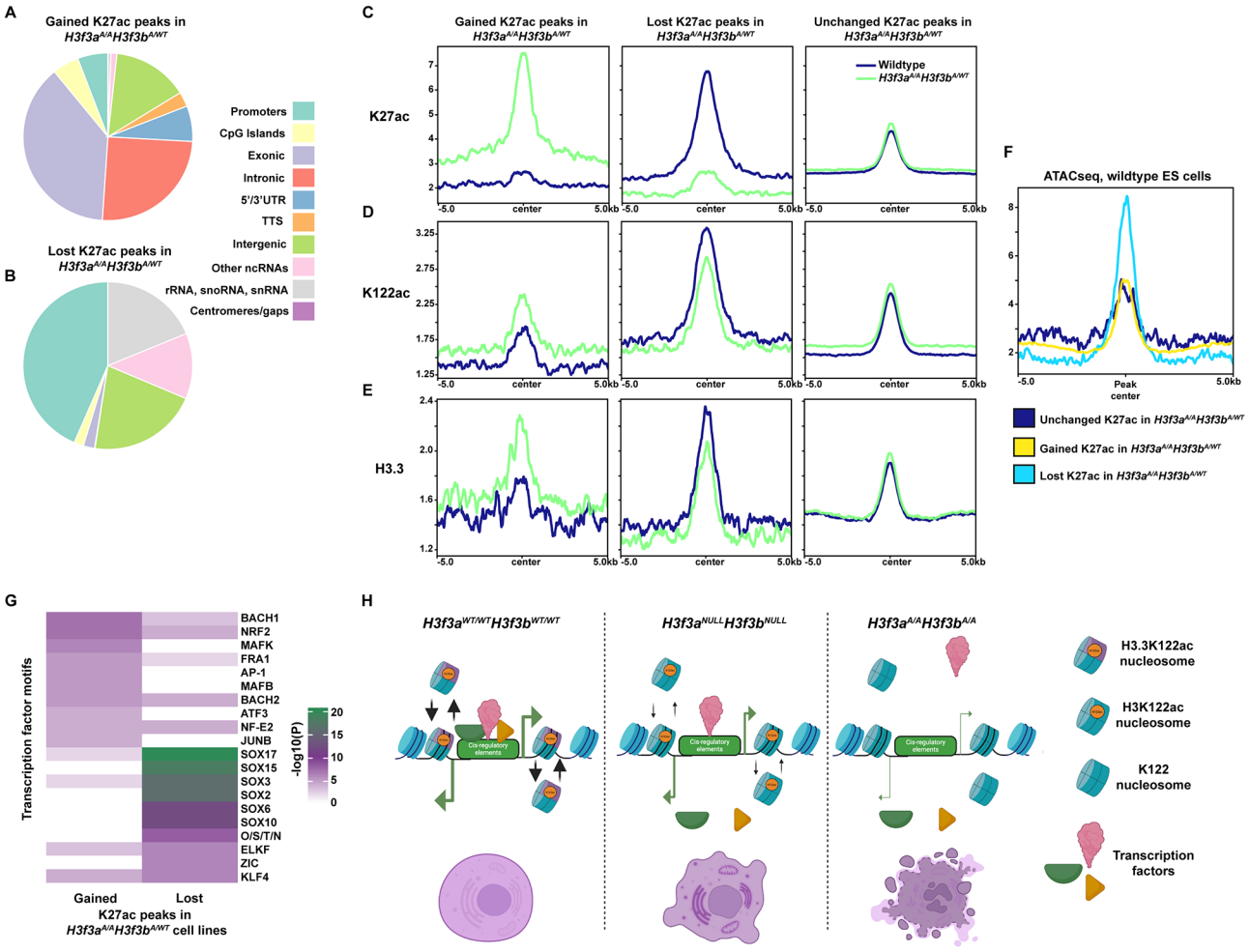

Fig. 6 H3 and H3.3 acetylation dynamics at putative enhancers in targeted and wildtype mES cells. **A**. Pie chart of the HOMER annotation of gained K27ac peaks in *H3f3a*$^{A/A}$*H3f3b*$^{A/WT}$ mES cells relative to wildtype. Each color corresponds to a genomic feature denoted in the legend (right). **B**. As in A, for lost K27ac peaks in *H3f3a*$^{A/A}$*H3f3b*$^{A/WT}$ mES cells relative to wildtype. **C**. K27ac enrichment in wildtype and *H3f3a*$^{A/A}$*H3f3b*$^{A/WT}$ mES cells over gained, lost, and unchanged TSS distal H3K27ac peaks from *H3f3a*$^{A/A}$*H3f3b*$^{A/WT}$ mES cell. **D**. As in C, for K122ac enrichment. **E**. As in C, for H3.3 enrichment. **F**. Wildtype mES cell ATAC-seq signal over gained, lost, and unchanged TSS distal H3K27ac peaks from *H3f3a*$^{A/A}$*H3f3b*$^{A/WT}$ mES cells. **G**. Top 10 most enriched TF motifs found at TSS distal H3K27ac peaks gained or lost in *H3f3a*$^{A/A}$*H3f3b*$^{A/WT}$ mES cells relative to wildtype. Color indicates -log10(*P*) as defined by HOMER. **H**. Model for how H3.3K122A may result in lethality in mES cells

wildtype mES cells relative to gained or unchanged peaks (Fig. 6C-F). Gained and lost TSS distal K27ac peaks displayed the expected changes in K27ac and K122ac enrichment in *H3f3a*$^{A/A}$*H3f3b*$^{WT/A}$ mES cells (Fig. 6C, D), suggesting that these are putative enhancers with altered activity in the *H3f3a*$^{A/A}$*H3f3b*$^{WT/A}$ mES cells. Interestingly, gained TSS distal K27ac peaks exhibited an increase in H3.3 levels while lost peaks exhibited a reduction but still maintained H3.3 enrichment (at levels similar to gained or unchanged peaks; Fig. 6E). As with the promoter profiles, these changes in enrichment likely reflect changes in transcription activity. Using the K27ac TSS-distal differential peaks as input into motif analysis, we found that peaks lost in the *H3f3a*$^{A/A}$*H3f3b*$^{WT/A}$ cell lines were strongly enriched for motifs associated with regulation of pluripotency (including SOX family motifs and the OCT4/SOX2/NANOG/TCF motif; Fig. 6G). These motifs did not have a robust enrichment at promoter distal K27ac peaks gained in *H3f3a*$^{A/A}$*H3f3b*$^{WT/A}$ cell lines (Fig. 6G). Together, these analyses suggest that the H3.3K122A mutation influences the activity of a subset of putative enhancers in mES cells, and this may contribute to the mRNA transcription changes and pluripotency defects observed in the *H3f3a*$^{A/A}$*H3f3b*$^{WT/A}$ mES cell lines.

Discussion

The role of H3.3 in mES cells has been extensively characterized, showing that H3.3 and its associated posttranslational modifications are important for the regulation of

endogenous retroviruses, heterochromatin, global H3 acetylation, and facilitating differentiation [7, 9, 10, 13, 16, 18, 19, 33, 34]. Past studies also demonstrate that H3.3 is dispensable for proper transcription and regulation of pluripotency in mES cells. Specifically, depletion or deletion of H3.3 is not associated with proliferation defects, reduction in pluripotency, or strong transcriptional phenotypes [10, 13, 18, 33], arguing that the effects we observe are not due to reduced levels of H3.3 and are rather attributed to the H3.3K122A mutants.

Our findings highlight an importance for H3.3K122 in viability and maintenance of mES cells, but the exact mechanism remains elusive. *H3f3a*$^{A/A}$*H3f3b*$^{WT/A}$ mES cells still acquire K27ac and K122ac in a transcription-dependent manner, arguing that this residue does not regulate H3K27 acetylation dynamics as has been shown for H3.3S31P [13]. Our findings indicate that differences in the activity of putative enhancers between *H3f3a*$^{A/A}$*H3f3b*$^{WT/A}$ and wildtype mES cells may play a role in the observed transcriptional defects of the targeted cell lines. Incorporation of H3.3 at regions of active transcription promotes nucleosome turnover, which is important for TF binding, histone modification maintenance, and proper regulation of transcription [1, 2]. Likewise, H3K122ac promotes nucleosome eviction in vitro and is necessary for rapid transcription activation in *S. pombe* and H3K122 promotes nucleosome occupancy over highly transcribed genes in *S. cerevisiae* [22, 24]. Therefore, H3.3K122 may play an important role in H3.3 turnover dynamics and the H3.3K122A mutation may disrupt this process. We envision that, whereas mES cells lacking H3.3 have less nucleosome turnover but still enough for viability through incorporation of H3.1/2 in the place of H3.3, in cells expressing H3.3K122A, H3.3K122A is incorporated into nucleosomes but disrupts nucleosome turnover to point that the result is lethality (Fig. 6H). The correlation between the number of targeted *H3f3* alleles and severity of phenotypes observed in mutant cell lines supports this model, but further studies are required.

Methods

Cell culture

ES-E14TG2a (E14) mES cells from male *Mus musculus* origin (RRID: CVCL9108361 [35]) were cultured as previously described [36] at 37 °C and 5% CO_2 in DMEM base medium (Sigma Aldrich) supplemented with 10% FBS (Sigma Aldrich), 1X non-essential amino acids (Corning), 2mM L-glutamine (Corning), β-mercaptoethanol (Acros Organics) and LIF on 10 cm plates precoated with 0.2% gelatin. For LIF+2i media, LIF media was further supplemented with 3 μM CHIR99021 GSK inhibitor (p212121), and 1 μM PD0325091 MEK inhibitor (p212121). Cells were passaged every ~48 h using trypsin and split at a ratio of ~1:8 with fresh medium. Routine anti-mycoplasma TC hood cleaning was conducted (LookOut DNA Erase spray, Sigma Aldrich) and cell lines were screened to confirm no mycoplasma presence. While generating clones, cells were grown in media with the addition of 1X penicillin/streptomycin (Corning) to prevent bacterial contamination.

Guide RNA cloning

Homology constructs for *H3f3a* and *H3f3b* (Supplemental Table 3) were designed to mutate residue 122 from lysine to alanine and mutate the PAM sequence (both highlighted in red). Oligos generated for the *H3f3a* or *H3f3b* gRNA were phosphorylated and annealed, then ligated to the px330-puro plasmid backbone using a simultaneous Fast Digest *Bbs1* (ThermoFisher) digestion and Quick Ligase ligation (NEB). Plasmids were purified using the GenElute HP Plasmid Maxiprep Kit (Sigma Aldrich) following the manufacturer's instructions and confirmed using Sanger sequencing (Genewiz).

Homology constructs were synthesized using IDT gBlocks Gene Fragments (IDT). The lyophilized construct was resuspended in 5 μL of nuclease-free water and 1 μL was used to clone the construct into the TOPO vector using the Zero Blunt TOPO PCR Cloning Kit for Sequencing (ThermoFisher) according to the manufacturer's directions. The resulting plasmids were purified using the GenElute HP Plasmid Maxiprep Kit (Sigma Aldrich) and confirmed using Sanger sequencing (Genewiz).

H3.3K122A cell line generation

The targeting strategy used to generate cell lines where all four H3.3 alleles were mutated from lysine 122 to alanine is depicted in Fig. 1A. To generate cell lines, 2×10^5 cells were plated in a single well in a 6 well dish 24 h prior to transfection. One hour prior to transfection, medium was replaced with fresh, antibiotic-free medium. Three μg of pX330-puro Cas9/guide RNA vector and 3 μg of recombination template vector were combined in 100 μL of pre-warmed OptiMEM (Gibco). 24 μL of FuGENE HD (Promega) was added and the mixture was incubated at room temperature for 10 min. The mixture was added in drops evenly around the well of the dish and then gently swirled to ensure even distribution. 14–16 h post-transfection, cells were split using 0.5% trypsin (Gibco) and plated at varying densities on gelatinized 10 cm plates in antibiotic-free media. 48 h post-transfection, the media was replaced with media containing 2 μg/mL puromycin. 72 h post-transfection, the media was replaced with antibiotic-free media. Individual clones were picked 8

days post-transfection. Two days after picking clones, media was replaced with fresh penicillin/streptomycin media. Five days after picking clones, cells were split to 3 identical plates to allow for gDNA extraction and genetic screening and parallel storage for post-screening use. Targeting was performed in LIF and LIF + 2i containing media.

Clone screening

To extract gDNA, cells were washed once in 1xDPBS, lysed with ES cell lysis buffer (10 mM Tris pH 7.5, 10 mM EDTA, 10 mM NaCl, and 0.5% sarkosyl in water) including 1 mg/mL Proteinase K, and incubated overnight at 55 °C. The following day, plates were centrifuged for 2 min at 4 °C and 1000 rpm. DNA was precipitated using ice cold 100% ethanol with 75 mM NaCl and incubated for about 30 min until the solution cleared before centrifuging for 5 min at 4 °C and 3000 rpm. The supernatant was removed and the DNA was washed twice with 70% ethanol, then dried for an hour and resuspended in 50 µL 1X TE. PCR was performed on the extracted DNA in 96-well plates using primers that amplified the targeted *H3f3a* or *H3f3b* region (see Supplemental Table 2).

esiRNA generation and knockdown

Endoribonuclease-digested short interfering RNAs (esiRNAs) were generated as previously described [36]. An ideal target DNA sequence was identified within *H3f3b* and screened for unique nucleotide sequence via DEQOR. Amplified cDNA from wildtype mES cells was in vitro transcribed using T7 RNA polymerase. To generate esiRNAs, IVT products were digested with ShortCut RNase III (NEB) and purified using a PureLink RNA Mini Kit (Invitrogen). Transient transfections to deplete *H3.3b* were performed on wildtype cells (control for transfection efficiency) or *H3f3a* K122A clones on 6 wells using 5 µL of Lipofectamine 3000 (ThermoFisher) and 900 ng of esiRNAs for 48 h. Cells were harvested and counted with trypan blue on a BioRad Cell Counter. Following RNA isolation, depletion was quantified using RT-qPCR.

CRISPRi

A guide RNA for *H3f3a* was cloned into dCas9-KRAB-MeCP2 plasmid (Addgene 110821), as previously described [37]. dCas9-KRAB-MeCP2 was a gift from Alejandro Chavez & George Church (Addgene plasmid #110821; RRID: Addgene 110821). Plasmids were transfected into wildtype mES cells (control for transfection efficiency and CRISPRi activity) or *H3f3b* K122A clones on 6 wells using 5 µL of Lipofectamine 3000 (ThermoFisher), 5 µL of p3000 reagent, and 5 µg of plasmid for 48 h. Cells were harvested and counted with trypan blue on a BioRad Cell Counter. Following RNA isolation, transcript abundance was quantified using RT-qPCR.

Protein extraction and western blot analysis

For each protein, the following primary/secondary antibodies and dilutions were used: H3 (abcam: ab1791, lot GR300978-2, 1:1000), H3.3 (Millipore: 09-838, lot 3987735, 1:1000), K122ac (Invitrogen: PA5-112508, lot YJ4090633A, 1:1000), and ACTIN (Sigma: A1978, lot 037M4782V, 1:5000), IRDye 800CW Goat anti-rabbit IgG Secondary (LI-COR: 926-32211, 1:10000), and IRDye 800CW Goat anti-mouse IgG Secondary (LI-COR: 926-32210, 1:10000).

Cells were trypsinized and collected in a 15 mL conical tube, then centrifuged at 600 rcf for 5 min at 4 °C. Cell pellets were washed twice with cold 1XPBS and protein was extracted using 200 µL Triton Extraction Buffer (PBS containing 0.5% Triton X 100 (v/v), 2 mM phenylmethylsulfonyl fluoride (PMSF), 0.02% (w/v) NaN3). Concentration was determined using the Pierce BCA protein assay kit (ThermoFisher), and 7.5–10 µg protein per sample was loaded onto 15% Tris-acrylamide gels with Precision Plus ladder (Biorad). Gels were run for 40 V for 1 h, 120 V for 2.5 h, and then transferred at 20 V overnight to a nitrocellulose membrane (Biotrace). Successful transfer assessed using REVERT 700 total protein stain (LI-COR) and membranes were blocked using Intercept blocking buffer (LI-COR). Primary antibody incubations were conducted overnight at 4 °C, and secondary antibody incubations were conducted for 2 h at room temperature. All imaging was performed using a LI-COR Odyssey DLx Imager according to the manufacturers specifications. Protein quantification was conducted using ImageJ [38]. For total protein quantification, identical areas for each lane were selected and the mean pixel intensity was measured and subtracted from the mean pixel background intensity. For target protein quantification, identical size areas immediately surrounding the target band were selected and mean pixel intensity was measured and subtracted from mean background pixel intensity. Target protein quantification was then made relative to total protein quantification, and then made relative to wildtype. Three biological replicates were conducted per target for each cell line.

Cell growth assay

Cells were plated in 6 wells at a density of 50,000 cells per well. At days 1, 2, 3, 4, and 6 post-plating, cells were trypsinized using 0.5 mL of trypsin and stopped with 1.5 mL of ES cell medium. After achieving single cell suspension, cells were counted on a TC20 cell counter (BioRad) using trypan blue stain to distinguish live cells. Three biological replicates were conducted for each cell line.

Alkaline phosphatase staining

Cells were washed twice in 1X Dulbecco's Phosphate-Buffered Saline (DPBS, Gibco) and crosslinked for five minutes at room temperature using 1% formaldehyde (Fisher) in DPBS. Crosslinking was quenched using 500 mM glycine and cells were washed using 1X DPBS twice. Cells were stained using Vector Red Alkaline Phosphatase Staining Kit (Vector Labs) per manufacturer's instructions in a 200 mM Tris-HCl buffer, pH 8.4. 2 mL working solution was added to each 6 well and incubated in the dark for 30 min before being washed with 1XPBS and imaged. Three biological replicates were conducted for each cell line.

4sU-labelling and RNA isolation

4sU-labelled RNA was generated and isolated from cells using TT-seq as previously described [28, 39]. Media was aspirated from cell plates and replaced with 10 mL of 500 nM 4-thiouridine (4sU, Carbosynth T4509) containing ES cell media and the plates incubated at 37 °C with 5% CO_2 for 5 min. After 5 min, the 4sU-containing media was aspirated and the cells were washed with 1xPBS and 2 mL TRIzol (Invitrogen) was added directly to the plate. Cell lysate were collected, and RNA was extracted according to ThermoFisher's recommendations. RNA concentration was determined by Qubit with the Qubit RNA broad range quantification kit (ThermoFisher). 100 µg of total RNA was diluted to a concentration of 240 ng/µL at a volume of 416.67 µL in 1XTE and then fragmented with a Diagenode Bioruptor Pico on high power for one 30 s cycle. The fragmented RNA was then combined with 283.33 µL 1XTE, 100 µL 10X Biotinylation buffer (100 mM Tris pH 7.4 and 10 mM EDTA), and 200 µL of 1 mg/mL biotin-HPDP (ThermoFisher) in dimethylformamide (DMF; freshly prepared). Samples were vortexed, then incubated in a thermomixer at 37 °C shaking at 1000 RPM in the dark for 2 h. Samples were chloroform extracted, isopropanol/salt precipitated, and resuspended in 22 µL of nuclease-free water. Sixty uL of Streptavidin C1 beads (Invitrogen) were prepared for RNA separation by washes with 1 mL of 1 M NaOH and 50 mM NaCl and resuspended in 60 µL of TT-seq Binding buffer (10 nM Tris pH 7.4, 300 mM NaCl, 0.1% Triton). Then, 60 µL of prepared streptavidin C1 beads were added to each sample and rotated at room temperature for 20 min. Following incubation, the samples were magnetized for 1 min and the supernatant (containing the unlabeled RNA) was placed in a separate 1.5 mL tube and put on ice. The unlabeled RNA from the supernatant was Phenol: Chroloform: Isopropanol(PCI)/chloroform extracted, isopropanol/salt precipitated, and resuspended in 100 µL of nuclease-free water. The bead-bound labeled nascent RNA was washed twice with 500 µL of High Salt buffer (50 mM Tris pH 7.4, 2 M NaCl, 0.5% Triton), twice with 500 µL of TT-seq Binding buffer, and once with 500 µL of Low Salt buffer (5 mM Tris pH 7.4, 0.1% Triton), rotating for 1 min at room temperature, re-magnetizing and resuspending the beads during each wash. The nascent RNA was recovered from the beads through two rounds of 100 µL of freshly prepared 100 mM DTT and incubating in a thermomixer at 65 °C and 1000 RPM shaking for 5 min. Eluted nascent RNA was recovered with a PCI extraction and an isopropanol/salt/glycogen precipitation. RNA pellets were resuspended in 25 µL of nuclease-free water. The total RNA and nascent RNA from each sample were used for RT-qPCR and TT-seq libraries as described below.

Transient transcriptome sequencing (TT-seq)

For TT-seq, three replicates for wildtype mES cells, and one replicate for each mutant cell line were performed. 4sU labelling for TT-seq was performed as described in 4sU labelling section. RNA pellets were resuspended in 1X TE buffer, at approximately 100 µL per 100 µg of RNA. Strand-specific nascent RNA library building was performed as previously described [39] using the NEBNext Ultra II Directional Library kit with the following changes: The rRNA depleted RNA was fragmented at 94 °C for fifteen minutes following the manufacturer's instructions for intact RNA, the fragmentation, first strand cDNA synthesis, and second strand cDNA synthesis were performed at double the reaction volume in the manufacturer's instructions, the adaptors were diluted 1:5 in Adaptor Dilution Buffer, the primers were diluted 1:5 in nuclease-free water, and 7 cycles of PCR were used to amplify the libraries. Finished libraries were quantified by Quibit with the dsDNA High Sensitivity kit and run on a Fragment Analyzer to confirm high quality of each library prior to sequencing. Libraries were sequenced paired-end on an Illumina NextSeq500 to ~40 million mapped reads.

TT-seq analysis

Raw paired end fastq files were analyzed with fastQC [40] using default parameters to ensure high data quality and adapter sequences were trimmed using cutadapt [41]. Reads were aligned with the mm10 Gencode annotation (GRCm38.p6, vM23) using STAR [42] with the following parameters: outFilterMismatchNoverReadLmax 0.02, outFilterMultimapNmax (1) samtools [43] was used to filter reads and generate indexed bams with the following parameters: -q 7 -f (2) Feature counts were generated using featurecounts [44] options -B -t "exon" -g "gene_name" -F GTF -p -s 2 with the mm10 (GRCm38.p6, vM23) genome annotation (GTF format). Differential gene expression analysis was conducted using DEseq2 [45] with cutoff as $|\log2(FC)| \geq 0.75$ and FDR ≤ 0.05. Gene Ontology analysis on gene sets of interest was performed

the R package "clusterProfiler" [46] using all Gencode features as background. Upset plots were generated using the R package "upsetR" (https://github.com/hms-dbmi/UpSetR), and volcano plots were generated using R package "EnhancedVolcano" (https://bioconductor.org/packages/release/bioc/html/EnhancedVolcano.html).

Reverse transcription and quantitative PCR (RT-qPCR)

cDNA was generated from 1 µg of total RNA or 100 ng of 4sU labelled RNA with random hexamers (Promega) with homemade reverse transcriptase (RT). Generated cDNA was used as a template in qPCR reactions using 2X SYBR FAST mix (KAPA) and 5 µM target specific primers (see Supplemental Table 2) on a Lightcycler 96 (Roche). Target transcript abundance in samples was determined using the ΔΔCT normalization method relative to wildtype samples, using *Gapdh* transcript abundance for internal normalization as previously described [47].

CUT&RUN

The following antibodies and dilutions were used for CUT&RUN: H3.3 (Active Motif 91191, lot # 01022005; 1:50), K122ac (Invitrogen PA5-105108, lot # WJ3411065A; 1:50), and K27ac (abcam ab4729, lot # GR3416784-1; 1:100).

CUT&RUN was performed as described [39, 48, 49] using recombinant ProteinA-MNase (pA/G-MN) or Protein A/Protein G-MNase (pA/G-MN), as specified. For each target, two replicates for wildtype and one replicates for each mutant cell line were performed. Briefly, 100,000 nuclei were isolated from cell populations using a hypotonic buffer (20 mM HEPES-KOH, pH 7.9, 10 mM KCl, 0.5mM spermidine, 0.1% Triton X-100, 20% glycerol, freshly added protease inhibitors) and flash frozen. Nuclei were thawed and bound to lectin-coated concanavalin A magnetic beads (50 µL bead slurry per 100,000 nuclei; Polysciences). Immobilized nuclei were pre-blocked with blocking buffer (20 mM HEPES, pH 7.5, 150 mM NaCl, 0.5mM spermidine, 0.1% BSA, 2 mM EDTA, fresh protease inhibitors) and washed in wash buffer (20 mM HEPES, pH 7.5, 150 mM NaCl, 0.5mM spermidine, 0.1% BSA, fresh protease inhibitors). Nuclei were incubated in wash buffer containing primary antibody (H3.3, K122ac, K27ac) overnight at 4 °C with rotation. Nuclei were incubated in wash buffer containing primary antibody for 1 h at room temperature with rotation. Next, samples were washed twice with wash buffer and incubated in wash buffer containing recombinant pA-MN (for K122ac, K27ac) or pA/G-MN (for H3.3) for 30 min at room temperature with rotation. Controls lacking a primary antibody were subjected to the same conditions but incubated in wash buffer without any primary antibody prior to incubation with pA-MN/pA/G-MN. After incubation, samples were washed twice with was buffer and equilibrated to 0 °C in an ice/water bath. MNase cleavage was activated upon addition of 3 mM $CaCl_2$. Digestion was chelated for samples containing primary antibody K27ac, after 30 min on the ice water bath, using 20 mM EDTA, 4 mM EGTA, 200 mM NaCl, and 1.5 pg MNase-digested *S. cerevisiae* mononucleosomes were added as a spike-in control. Genomic fragments were released after an RNase A treatment. Released fragments were separated through centrifugation. Digestion was chelated for samples containing primary antibodies K122ac and H3.3 after 30 min on the ice water bath, using a low-salt treatment: 10 mM EDTA, 2 mM EGTA, 150 nM NaCl, 5 mM TritonX, and 1.5 pg MNase-digested S. cerevisiae mononucleosomes were added as a spike-in control. Genomic fragments were released after being incubated for 1 h at 4 °C and released fragments were separated from beads. The salt concentration of low salt treated samples were increased to 500 mM and additional RNase A.

Isolated fragments from all samples were used as input for a library build consisting of end repair and adenylation, adapter ligation, and subsequent purification with AMPure XP beads (Agencourt). Barcoded fragments were then amplified by 15 cycles of high-fidelity PCR and purified using agarose gel extraction. Libraries were pooled and sequenced on an Illumina NextSeq500 to a depth of ~ 10 million mapped reads.

CUT&RUN analysis

Paired-end fastq files were trimmed to 25 bp and mapped to the mm10 genome with bowtie2 [50] (options -q -N 1 -X 1000). Mapped reads were duplicate-filtered using reads with insufficient mapping quality (MAPQ ≥ 10) were removed using samtools [43]. Reads were converted to bigWig files using deepTools [51] with the spike in *S. cerevisiae* mapped reads used as a scaling factor. Heatmaps and metaplots were generated using deepTools. Peaks were called from CUT&RUN samples using MACS2 [52] with no antibody samples as input. For each target, peaks from all samples were combined to create a consensus peak set. After removing all peaks with less than 10 counts in 50% of samples, differential enrichment peak analysis was performed using edgeR [53] for all available replicates of each condition with RUVseq [54] correction. Differentially enriched peaks were defined as $|\log_2(FC)| \geq 0.5$ and FDR ≤ 0.05. For each target, samples peak annotations and motif enrichment analysis were performed using HOMER [55].

Supplementary Information

The online version contains supplementary material available at https://doi.org/10.1186/s13072-024-00557-3.

Supplementary Material 1

Acknowledgements
We thank members of the Hainer Lab for critical comments, discussion, and feedback regarding this article. This work was supported by the NIH grant R35GM133732 (to S.J. Hainer) and NSF GRFP (to B. J. Patty). This project used the University of Pittsburgh HSCRF Genomics Research Core, RRID: SCR_018301 NextSeq2000, with special thanks to the assistant director, Will MacDonald. This research was supported in part by the University of Pittsburgh Center for Research Computing, RRID: SCR_022735, through the resources provided. Specifically, this work used the HTC cluster, which is supported by NIH award number S10OD028483.

Author contributions
Conceptualization: BJP, SJH; Methodology: BJP, CJ, SML, KT, SJH; Writing – original draft: BJP, SJH; Writing – revised draft: SJH; Funding acquisition: SJH; Supervision: SJH; Project administration: SJH. All authors reviewed the manuscript.

Funding
This work was supported by the NIH grant R35GM133732 (to SJH) and a NSF GRFP (to BJP).

Data availability
We have placed all the data on GEO, accession numbers GSE272575 (TT-seq) and GSE272577 (CUT&RUN).

Declarations

Ethics approval and consent to participate
Not applicable.

Consent for publishing
The manuscript has been read and approved by all named authors.

Competing interests
The authors declare no competing interests.

Received: 30 July 2024 / Accepted: 24 October 2024
Published online: 01 November 2024

References

1. Martire S, Banaszynski LA. <ArticleTitle Language="En">The roles of histone variants in fine-tuning chromatin organization and function. Nat Rev Mol Cell Biol. 2020;21:522–41.
2. Talbert PB, Henikoff S. Histone variants at a glance. J Cell Sci. 2021;134:1–10.
3. Bramlage B, Kosciessa U, Doenecke D. Differential expression of the murine histone genes H3.3A and H3.3B. Differentiation. 1997;62:13–20.
4. Tang MCW, et al. Contribution of the Two Genes Encoding Histone Variant H3.3 to Viability and Fertility in Mice. PLoS Genet. 2015;11:1–23.
5. Muhire BM, Booker MA, Tolstorukov MY. Non-neutral evolution of H3.3-encoding genes occurs without alterations in protein sequence. Sci Rep. 2019;9:1–11.
6. Klein RH, Knoepfler PS. Knockout tales: the versatile roles of histone H3.3 in development and disease. Epigenetics Chromatin. 2023;16:1–8.
7. Banaszynski LA, et al. Hira-dependent histone H3.3 deposition facilitates prc2 recruitment at developmental loci in ES cells. Cell. 2013;155:107–20.
8. Kori Y, et al. Multi-omic profiling of histone variant H3.3 lysine 27 methylation reveals a distinct role from canonical H3 in stem cell differentiation. Mol Omi. 2022;18:296–314.
9. Carraro M, et al. DAXX adds a de novo H3.3K9me3 deposition pathway to the histone chaperone network. Mol Cell. 2023;83:1075–e10929.
10. Tafessu A, et al. H3.3 contributes to chromatin accessibility and transcription factor binding at promoter-proximal regulatory elements in embryonic stem cells. Genome Biol. 2023;24:1–23.
11. Tagami H, Ray-Gallet D, Almouzni G, Nakatani Y, Histone. H3.1 and H3.3 Complexes Mediate Nucleosome Assembly Pathways Dependent or Independent of DNA Synthesis. Cell. 2004;116:51–61.
12. Xue Y et al. The ATRX syndrome protein forms a chromatin-remodeling complex with Daxx and localizes in promyelocytic leukemia nuclear bodies. *Proc. Natl. Acad. Sci. U. S. A.* 100, 10635–10640 (2003).
13. Martire S, et al. Phosphorylation of histone H3.3 at serine 31 promotes p300 activity and enhancer acetylation. Nat Genet. 2019;51:941–6.
14. Fosslie M, et al. Going low to reach high: Small-scale ChIP-seq maps new terrain. Wiley Interdiscip Rev Syst Biol Med. 2020;12:1–24.
15. Maze I, et al. Critical Role of Histone Turnover in Neuronal Transcription and Plasticity. Neuron. 2015;87:77–94.
16. Deaton AM, et al. Enhancer regions show high histone H3.3 turnover that changes during differentiation. Elife. 2016;5:1–24.
17. Kraushaar DC et al. Genome-wide incorporation dynamics reveal distinct categories of turnover for the histone variant H3.3. Genome Biol 14, (2013).
18. Fang HT et al. Global H3.3 dynamic deposition defines its bimodal role in cell fate transition. Nat Commun 9, (2018).
19. Elsässer SJ, Noh KM, Diaz N, Allis CD, Banaszynski LA, Histone. H3.3 is required for endogenous retroviral element silencing in embryonic stem cells. Nature. 2015;522:240–4.
20. Claringbould A, Zaugg JB. Enhancers in disease: molecular basis and emerging treatment strategies. Trends Mol Med. 2021;27:1060–73.
21. Wang Y, Zhang C, Wang Y, Liu X, Zhang Z. Enhancer RNA (eRNA) in Human Diseases. Int J Mol Sci. 2022;23:1–19.
22. Tropberger P, et al. Regulation of transcription through acetylation of H3K122 on the lateral surface of the histone octamer. Cell. 2013;152:859–72.
23. Manohar M, et al. Acetylation of histone H3 at the nucleosome dyad alters DNA-histone binding. J Biol Chem. 2009;284:23312–21.
24. Hainer SJ, Martens JA. Identification of histone mutants that are defective for transcription-coupled nucleosome occupancy. Mol Cell Biol. 2011;17:3557–68.
25. Hyland EM, et al. Insights into the Role of Histone H3 and Histone H4 Core Modifiable Residues in Saccharomyces cerevisiae. Mol Cell Biol. 2005;25:10060–70.
26. Pradeepa MM, et al. Histone H3 globular domain acetylation identifies a new class of enhancers. Nat Genet. 2016;48:681–6.
27. Štefková K, Procházková J, Pacherník J. Alkaline phosphatase in stem cells. *Stem Cells Int.* 2015, (2015).
28. Schwalb B, et al. TT-seq maps the human transient transcriptome. Sci (80-). 2016;352:1225–8.
29. Martin BJE, et al. Transcription shapes genome-wide histone acetylation patterns. Nat Commun. 2021;12:1–9.
30. Wang Z, et al. Combinatorial patterns of histone acetylations and methylations in the human genome. Nat Genet. 2008;40:897–903.
31. ALLFREY VG, FAULKNER R, MIRSKY AE. Acetylation and Methylation of Histones and Their Possible Role in the. *Proc. Natl. Acad. Sci. United States* 51, 786–794 (1964).
32. Morgan MAJ, Shilatifard A. Reevaluating the roles of histone-modifying enzymes and their associated chromatin modifications in transcriptional regulation. Nat Genet. 2020;52:1271–81.
33. Yang Y, et al. HIRA complex presets transcriptional potential through coordinating depositions of the histone variants H3.3 and H2A.Z on the poised genes in mESCs. Nucleic Acids Res. 2022;50:191–206.
34. Wong LH, et al. ATRX interacts with H3.3 in maintaining telomere structural integrity in pluripotent embryonic stem cells. Genome Res. 2010;20:351–60.
35. Risch N, et al. HPRT -deficient (Lesch-Nyhan) mouse embryos derived from germline colonization by cultured cells. Jr Archs gen Psychiat. 1981;20:753–8.
36. Klein DC, Troy K, Tripplehorn SA, Hainer SJ. The esBAF and ISWI nucleosome remodeling complexes influence occupancy of overlapping dinucleosomes and fragile nucleosomes in murine embryonic stem cells. BMC Genomics. 2023;24:1–16.
37. Yeo NC, et al. An enhanced CRISPR repressor for targeted mammalian gene regulation. Nat Methods. 2018;15:611–6.
38. Robinson BP, et al. Alpha-arrestins Aly1/Art6 and Aly2/Art3 regulate trafficking of the glycerophosphoinositol transporter Git1 and impact phospholipid homeostasis. Biol Cell. 2022;114:3–31.
39. Klein DC, Lardo SM, McCannell KN, Hainer S. J. FACT regulates pluripotency through distal regulation of gene expression in murine embryonic stem cells. bioRxiv. 2022;454509. https://doi.org/10.1186/s12915-023-01669-0.
40. Andrews S. FastQC A Quality control tool for high throughput sequence data. Babraham Bioinfo 3–5 (2018).
41. Martin M. Cutadapt removes adapter sequences from high-throughput sequencing reads. EMBnet J. 2011;17:10.
42. Dobin A, et al. Ultrafast universal RNA-seq aligner. Bioinf 29. 2013;STAR:15–21.
43. Li H, et al. The Sequence Alignment/Map format and SAMtools. Bioinformatics. 2009;25:2078–9.

44. Liao Y, Smyth GK, Shi W, FeatureCounts. An efficient general purpose program for assigning sequence reads to genomic features. Bioinformatics. 2014;30:923–30.
45. Love MI, Huber W, Anders S. Moderated estimation of fold change and dispersion for RNA-seq data with DESeq2. Genome Biol. 2014;15:1–21.
46. Wu T, et al. clusterProfiler 4.0: A universal enrichment tool for interpreting omics data. Innovation. 2021;2:100141.
47. Rao X, Huang X, Zhou Z, Lin X. An improvement of the 2ˆ(-delta delta CT) method for quantitative real-time polymerase chain reaction data analysis. Biostat Bioinforma Biomath. 2013;3:71–85.
48. Hainer SJ, et al. Suppression of pervasive noncoding transcription in embryonic stem cells by esBAF. Genes Dev. 2015;29:362–78.
49. Patty BJ, Hainer SJ. Transcription factor chromatin profiling genome-wide using uliCUT& RUN in single cells and individual blastocysts. Nat Protoc. 2021;16:2633–66.
50. Langmead B, Salzberg SL. Fast gapped-read alignment with Bowtie 2. Nat Methods. 2012;9:357–9.
51. Ramírez F, Dündar F, Diehl S, Grüning BA, Manke T, DeepTools. A flexible platform for exploring deep-sequencing data. Nucleic Acids Res 42, (2014).
52. Zhang Y et al. Model-based analysis of ChIP-Seq (MACS). Genome Biol 9, (2008).
53. Robinson MD, McCarthy DJ, Smyth GK, edgeR. A Bioconductor package for differential expression analysis of digital gene expression data. Bioinformatics. 2009;26:139–40.
54. Risso D, Ngai J, Speed TP, Dudoit S. Normalization of RNA-seq data using factor analysis of control genes or samples. Nat Biotechnol. 2014;32:896–902.
55. Heinz S, et al. Simple Combinations of Lineage-Determining Transcription Factors Prime cis-Regulatory Elements Required for Macrophage and B Cell Identities. Mol Cell. 2010;38:576–89.
56. Patty BJ, Hainer SJ. Widespread impact of nucleosome remodelers on transcription at cis-regulatory elements. bioRxiv [Preprint]. 2024:589208. https://doi.org/10.1101/2024.04.12.589208
57. Seneviratne JA, Ho WWH, Glancy E, et al. A low-input high resolution sequential chromatin immunoprecipitation method captures genome-wide dynamics of bivalent chromatin. Epigenetics Chromatin. 2024;17:3.

Publisher's note